Dose-dependent cell-based assays in V-shaped microfluidic channels†

Cheuk-Wing Li, Jun Yang and Mengsu Yang*

Received 5th January 2006, Accepted 28th April 2006
First published as an Advance Article on the web 18th May 2006
DOI: 10.1039/b600058d

The capability of lab-on-a-chip technologies in controlling cell transportation, generating concentration gradients, and monitoring cellular responses offers an opportunity to integrate dose-dependent cell-based bioassays on a chip. In this study, we have developed microfluidic modules featured with channel components and sandbag structures for positioning biological cells within the microchip. We have demonstrated that by geometric modulation of the microchannel architectures, it is possible to immobilize individual cells at desired locations with controllable numbers, to generate defined concentration gradients at various channel lengths, and to improve the efficiency and reproducibility in data acquisition. The microfluidic module was used to exercise a series of cell-based assays, including the measurement of kinetics and dynamics of intracellular enzymatic activities, the analysis of cellular response under the stimulation of two chemicals with defined concentration profiles, and the study of laser irradiation effect on cellular uptake of photosensitizers. The results demonstrated the capabilities of the microfluidic module for simultaneously conducting multiple sets of dose-dependent, cell-based bioassays, and for quantitatively comparing responses of individual cells under various stimulations.

Introduction

Dose-dependent studies are often performed in many quantitative bioassays to determine the biological activity of a substance towards cells over time. Usually, a range of differing concentrations for each substance is prepared to evaluate the response of cells. However, it is common to observe combined effects, *i.e.* additivity, antagonism, potentiation and synergism, on cells that were concurrently exposed to more than one factor. To study combined effects of two factors such as two substances, two sets of serial dilution experiments are often prepared for comparison. For example, to evaluate the effect of a receptor antagonist against a growth factor on cell proliferation, two sets of increasing doses of the growth factor are prepared in the absence and the presence of the antagonist at a fixed concentration.[1] The antagonistic effect on proliferation is inspected by comparing between the two sets of responses. These types of experiments are usually time-consuming and labor-intensive, and also require large amount of costly reagents.

The capability of microfluidics in controlling cell transportation,[2–5] generating concentration gradients,[6–9] and conducting cell culture[10–13] offers an opportunity to integrate the tedious yet indispensable dose-dependent cell-based bioassays on a chip. By altering the shape of the conventional intersection (T), we have shown that a V-shaped geometric modulation could control cell docking behavior as well as the mixing length for solution homogenisation within microchannels. As a logical continuation from these findings, we have further established a microfluidic platform capable of performing multiple sets of dose-dependent bioassays simultaneously and comparing responses of individual cells under various stimulations quantitatively. We have demonstrated that by controlling the multiphase laminar flow with a V-shaped channel geometry, parallel operation and detection of two sets of cell-based bioassays (hereafter called two pipelines) could be executed within an effective size of 0.2 × 0.15 cm^2. About 100 single cell data points could be interrogated in each pipeline to ensure the representative description of dose response among cells. Efficient data acquisition in a single confocal scanning was accomplished by packing the two pipelines in close proximity, demonstrating the potential of the compact data arrangement approach for further multiplexing.

Department of Biology and Chemistry, City University of Hong Kong, 83 Tat Chee Avenue, Kowloon, Hong Kong SAR.
E-mail: bhmyang@cityu.edu.hk; Fax: 852 2194 2554; Tel: 852 2788 7797
† Electronic supplementary information (ESI) available: Fig. S1 Effects of geometric modulation on fluidic pressure profile. Fig. S2 Data reproducibility on T and V-shaped microdevices. Fig. S3 Effects of geometric modulation on gradient profile. Fig. S4 Repeated experiments in different cell-based assays. Table S1 Gradient characteristics and mixing length in differently shaped gradient components. See DOI: 10.1039/b600058d

Experimental

I. Reagents and cells

Standard Hank's balanced salt solution (HBSS) (H8264, Sigma, St. Louis, MO) was used to prepare two modified buffer solutions, HstCa-1 and HstCa-2. For HstCa-1, DMSO (10% final, Sigma) and Pluronic F-127 (0.002% final, P-3000, Molecular Probes Inc., Eugene, USA) were added while only Pluronic F-127 (0.002% final) was added for HstCa-2. The working solutions of calcein-AM (CAM), ethidium bromide (EB, Boehringer, Mannheim GmbH, Germany) and tetramethylrosamine (TMR) (Molecular Probes) were prepared in HBSS with further addition of DMSO (10% final) and Pluronic F-127 (0.002% final).

Obtained from the American Type Culture Collection, suspension HL-60 cells (human promyelocytic leukemia, diameter ~15 μm) were cultured with RPMI 1640 in sterile flask. Cells (5×10^6) were harvested 15 min before experiment and washed three times in HstCa-2 before loading.

II. Microchip fabrication

Rapid microdevice fabrication has been demonstrated by molding PDMS against a PCB master.[14,15] Designs for channel systems were generated in a CAD program (CorelDRAW 12.0, Corel Corporation, UK). 2400 dpi transparencies were produced by a commercial printer from the CAD files. Serving as photomasks, the transparencies were placed on top of a print circuit board (PCB, Kinsten glassepoxy single sided, Chiefskill, Taiwan) that was subsequently exposed by a standard PCB exposure unit (KVB-30 exposure unit, Chiefskill) for 80 s. Exposed PCB was incubated in a developing agent (Chiefskill) for 10 min, rinsed and wet etched with ferric chloride for 1 h. After etching, the PCB was thoroughly rinsed before the remaining photoresist was removed by acetone. The PCB master featured with microchannels (100 × 20 μm; $W \times H$) and sandbag microstructures (an averaged height of 4 μm ± 2 μm) was covered with degassed PDMS prepolymer (10 base: 1 curing agent, Sylgard 184, Dow Corning, Midland, MI) followed by an incubation at 75 °C for 1 h according to published protocol.[16] The cured PDMS replica was carefully peeled off, trimmed and oxidized in a plasma cleaner (PDC-3XG, Harrick Scientific, Ossining, NY) for 2 min together with another thin slab PDMS placing on a piece of cleansed glass slide. With vials punched by a circular hole puncher (3 mm in diameter), the replica was irreversibly sealed against the PDMS thin slab to form a microdevice (Fig. 1B).

III. Fluorescence image and data acquisition

Confocal laser-scanning microscope (LSM 510, Carl Zeiss GmbH, Germany) was used for image acquisition. An argon laser (488 nm) was used to excite EB, CAM with 505–530 emission filters while a helium-neon laser (543 nm, 3.5 mW) was used for TMR with 585–615 emission filter. Laser switch setting was employed in two-dye analysis to avoid signal cross-talk. Unless otherwise specified, confocal detector parameters were autoscaled. Concentration gradient profiles were analyzed by the native profiling tool in Zeiss LSM software while background subtracted signal intensity median of whole cells were acquired by GenePix Pro (4.0, Axon Instruments Inc., CA, USA).

IV. Compare cell docking and on-chip CAM staining between T and V cores

HL-60 cells (5×10^6) were washed for 3 times in HstCa-2 before loading into each microdevice by liquid level program (LLP) A (Table 1). After five-minute cell docking, on-chip cell staining was performed by LLP B and confocal image of each microdevice was captured after 10 min of CAM staining.

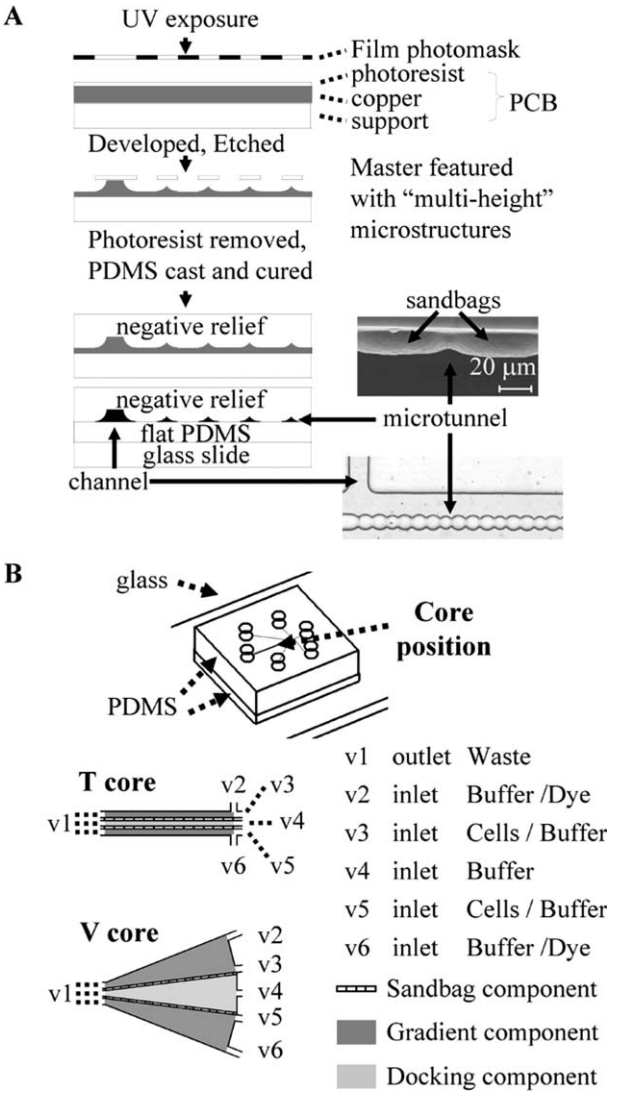

Fig. 1 (A) Schematic diagram for the fabrication of PDMS-based microfluidic structures based on a single step photolithography. Insets showed the microchannels, microtunnels and sandbag structures of the microdevice. See text for detail. (B) Design layout and vial designations of microdevice used in this study. The V core was comprised of sandbag, gradient and docking components. The outward pointing arrows depicted the common outlet v1 (waste) while other five inward pointing arrows were inlets named from v2 to v6. Corresponding liquid volume were loaded to these vials according to Table 1.

V. Compare EB concentration gradient profiles between T and V cores

For each microdevice, two snapshots of EB fluorescence images were acquired at five-minute intervals to evaluate the upper gradient component driven by LLP C (Table 1). LLP was switched to D and one more fluorescence image was taken after 5 min. Detection parameters were kept constant and Zeiss profiling tool was utilized to retrieve the intensity profiles along the white dotted line (Fig. 2B) as well as the buffer microchannel midline.

Table 1 Liquid level program (LLP) used in fluid manipulations

LLP	Operation mode	Liquid volume in individual vial (solution or buffer)/μL					
		v1	v2	v3	v4	v5	v6
A (load)	Cell docking	5[a]	20[a]	20 (cells)[b]	15[a]	20 (cells)[b]	20[a]
B (run)	CAM staining	5[c]	17 (CAM)[d]	17 (CAM)[d]	17 (CAM)[d]	17 (CAM)[d]	17 (CAM)[d]
C (run)	EB gradient	5[c]	17 (EB)[e]	17[a]	17[a]	17[a]	17[a]
D (run)	EB filled	5[c]	17 (EB)[e]	17 (EB)[e]	17 (EB)[e]	17 (EB)[e]	17 (EB)[e]
E (run)	1 factor	5[c]	17 (CAM)[f]	17[c]	17[c]	17[c]	17[c]
F (run)	2 factors, 2 varies	5[c]	17 (TMR)[g]	17[c]	17[c]	17[c]	17 (T_C)[h]
G (run)	2 factors, 1 varies	5[c]	17 (TMR)[g]	17[c]	17[c]	17[c]	17 (TMR)[g]

[a] HstCa-2. [b] Cells: HL-60 cells, cell density 5×10^6. [c] HstCa-1. [d] CAM: calcein-AM, 10 μM. [e] EB: ethidium bromide, 25 mM. [f] CAM: calcein-AM, 50 μM. [g] TMR: tetramethylrosamine, 10 μM. [h] T_C: mixture of tetramethylrosamine and calcein-AM, each 10 μM.

VI. On-chip conditioning 1: single factor in various concentrations and time points

Cells were docked according to liquid level program (LLP) A (Table 1) for 5 min. After the docking was completed, all vials were washed with HstCa-2 before switching to LLP E. With detector parameters kept constant throughout the experiment, confocal images were taken from 2.5 to 10 min. EB gradient profile was evaluated after the study.

A solution-based fluorescence assay was used to establish a control curve of CAM dose responses. Experiments were conducted by a microplate reader with autodispenser (PolarStar Optima, BMG Labtechnologies, USA). 100 uL of cells (2×10^6) and different volumes of buffer solution were manually loaded to the microplate wells. Then, complementary volumes of CAM solution were sequentially dispensed through the autodispenser so that total solution volume was 200 μL in each well. After each CAM dispensing, the microplate was shaken for 3 s followed by 3 min scanning. As a result, fifteen different CAM concentrations (excluding negative and solvent controls), ranging from 0–25 μM in HstCa-1, were examined in a 51 min period.

The origin of CAM signal fluctuation was evaluated by confocal imaging. In separated eppendorf tubes, HL-60 cells were incubated with CAM concentrations (3.75, 7.5, 10.0, 12.5, 19.0 μM) for 3 min before putting on a conventional slide and covered with glass slip. After 1 min, a confocal image was taken for each concentration and data were analysed by GenePix Pro software.

VII. On-chip conditioning 2: two factors, both in various concentrations

Cells were docked according to LLP A (Table 1) for 5 min and switched to LLP F after complete docking and washing. After 8 min, one confocal image was taken. EB gradient profile was evaluated after the study.

VIII. On-chip conditioning 3: two factors, one fixed while another in various concentrations

Cells were docked according to LLP A (Table 1) for 5 min and switched to LLP G after complete docking and washing. Then, docked cells on both sandbag components were incubated in identical TMR gradient for 7 min. An area within the black framework (Fig. 5A, top, ~1400 μm × 70 μm) of the upper sandbag component was further irradiated by helium-neon laser for 3 min in fast scan mode (scan rate: ~70 ms framework^{-1}). A confocal image was taken immediately after the laser irradiation. EB gradient profile was evaluated after the study.

IX. Simulation models

Diffusion coefficient of EB dye was retrieved according to literature.[17–19] EB gradient profiles in T and V-shaped structures were simulated by a commercial computational fluid dynamics (CFD) package (FLUENT 6.0, Fluent Inc, Lebanon, NH).[20,21] Each model was composed of grid patterns with ~300 000 nodes. Owing to the complicated geometry involved in the actual microdevice and limited computational power of the workstation used for modelling, the cross sectional dimension of a microtunnel was simplified as a regular triangle with 20 μm × 4 μm ($W \times H$) with referred to the SEM image in (Fig. 1A, inset). Fluidic flows were assumed as steady-state laminar flows whereas cell docking was assumed to have small impact on total flow quantity of the whole fluidic system.[3] Convergence criterions for all quantities (continuity, x-, y-, z-flow velocity and concentration of EB, CAM and TMR fluorophore) were 10^{-5}.

Simulated pressure and gradient profiles were exported to Excel software for further analysis together with the acquired experimental data. A macro was written by Visual Basic (6.0, Microsoft Corporation, USA) to compare all the acquired data points between experiments and theoretical models.

Results and discussion

Improving on the conventional T-shaped microchannel with a V-shaped geometry

Various cell-based assays have been carried out on microfluidic platforms, where biological cells were immobilized within a microdevice *via* different cell retention techniques.[3,5,14,22–33] We have previously described a cell docking method where a large number of suspension cells were immobilized in a controlled fashion on designated locations within a microchannel through fluid pressure differences.[3] We have also developed a "sandbag" structure for docking individual cells along a microchannel.[14] Here, we further explored the effects of microchannel geometry in maximizing the throughput of on-chip cell-based bioassays. The current knowledge in fluid mechanics has provided the basis to predict the effects on concentration gradient and pressure distribution

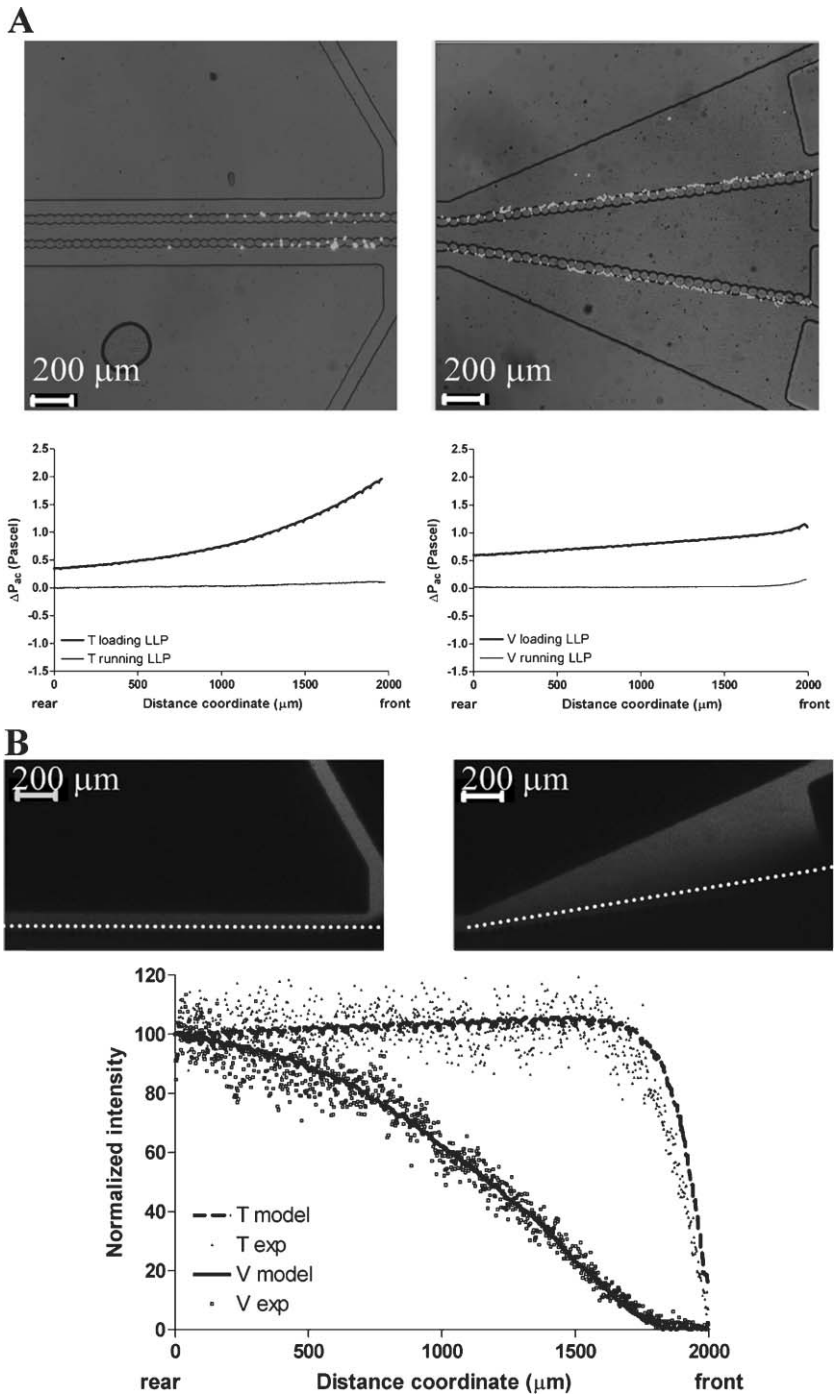

Fig. 2 (A) Experimental validation of geometric effects on docking capacity: Identical LLPs were applied to T and V cored microdevice and HL-60 cells were stained by calcein-AM after cell docking. (Left, T core) Only half of the sandbag components were docked with HL60 cells in the confocal image. Below the image were the corresponding CFD simulated pressure profiles of T cored microdevice at running and loading LLP. (Right, V core) Confocal image illustrated that sandbag components were fully populated and the corresponding CFD simulated pressure profiles of V cored microdevice were shown. The difference in docking capacity was representative of at least five experiments. (B) Experimental validation of geometric effects on mixing length: from the white dotted line in each core, EB gradient profile was retrieved and compared with the simulated profile interrogated at equivalent trajectory. Data were plotted underneath showing that the experimental and simulated gradient profiles were in good agreement.

profiles by altering the shape of microchannels. Hence, we fabricated two types of microdevices: a conventional T-shaped microdevice and its V-shaped analog and compared the potential of conducting single cell experiments on each device.

The PDMS-based microfluidic devices were fabricated by a single-step ''soft'' photolithography to construct multi-height microstructure with PCB prototyping (Fig. 1A).[14] The device was featured with ''sandbags'' (SEM image, inset of Fig. 1A),

which were constrictive microstructures for trapping biological cells at desired positions along the microchannels. The core layout of T and V microdevice was illustrated in Fig. 1B, where two gradient components were interconnected with a docking component by two sandbag structures. Different liquid volumes could be loaded into the access vials to create liquid level differences that were sufficient to generate fluidic flow within microchannels. The gradient profile and cell-docking capacity were predetermined by the V shape geometries under specific liquid level program (LLP) as tabulated in Table 1.

With schematics depicted in Fig. 1B, microdevices featured with T-shaped or V-shaped cores were fabricated for the evaluation of pressure distribution effect (Fig. 2A). Using liquid level program (LLP) A (Table 1, a loading LLP), mammalian HL-60 cells were docked on both sandbag components for 5 min with subsequent CAM staining by LLP B (a running LLP). Cell viability was confirmed by confocal fluorescence images after 10 min of on-chip staining (Fig. 2A, images). The total number of cells immobilized individually by the sandbag component, hereafter called docking capacity, was higher in the V core than in the T core. Corresponding plots of ΔP_{ac} *versus* distance coordinate were simulated (Fig. 2A, charts) (for details, please refer to Fig. S1†). Positive ΔP_{ac} values indicated that cells were driven hydrodynamically towards sandbag from gradient component. For each microdevice, the ΔP_{ac} profiles during loading and running LLP (Table 1) were simulated for comparison.

Although both T and V cores sustained minimal fluidic stress during running LLP, their ΔP_{ac} profiles were considerably different at loading LLP (Fig. 2A, charts). The partial V-shaped enlargement exhibited a mild drop of ΔP_{ac} along distance coordinate as comparing with the T-shaped channel. The difference in pressure profiles leaded to different docking capacity within the microdevices (Fig. 2A, images), where the T core showed an empty sandbag rear in contrast to the fully populated sandbag in V core. It is obvious that ΔP_{ac} in T core has steeply dropped below the threshold required for cell docking at sandbag rear positions. For the T core, docking was attempted at increasing liquid pressure but resulted in the cell squeezing through the sandbag near the front positions. By tuning fluidic pressure profile with V-shaped geometry, ΔP_{ac} along the entire sandbag was sustained to achieve full docking. The tuning effect of V-shaped geometry was associated with partial channel enlargement of gradient and docking components. (see also Fig. S1D, identical geometry of gradient and docking components were required to improve docking capacity.†) V-shaped geometric modulation may also find its applications in trapping other particle entities, such as beads, along microchannels.

This simple V-shaped geometry modulated not only pressure distribution but also concentration gradient profiles. In order to validate this effect, both T and V cored microdevices were tested with ethidium bromide (EB) (LLP C, Table 1). For each microdevice, experimental and simulated gradient profiles were retrieved along the white dotted trajectories depicted in Fig. 2B, images. As shown, V-shaped geometry extended the mixing length with increased gradient concentrations over distance while the T-shaped control exhibited an early gradient plateau. Mixing length and gradient profiles of T and V cores agreed well with simulated results (Fig. 2B, chart) while data reproducibility ($N = 5$) was confirmed in Fig. S2.† It should also be noted that the mixing length could be regulated by the degree of V-shaped geometry (see also Fig. S3†). Obviously, the extended mixing length in the V core allowed the distribution of a greater distance of gradient concentrations over more docked cells. Therefore, there is greater potential to perform high throughput single cell experiments in the V core when comparing with the conventional T analog. This is demonstrated by several cell-based assays carried out on the V cored microfluidic device below.

Cell-based assays on dual V-shaped microdevice

In a comparative study, it is ideal to keep all experimental parameters at constant, except for the factor(s) of interest. We have designed the microfluidic platform such that identical microenvironment could be easily attainable by a replicating microchannel architecture of V-shaped geometries. Taking one gradient and sandbag component as a pipeline, one set of dose-dependent bioassays could be conducted by generating a continuum of analyte concentrations along a sandbag component populated with cells. In order to eliminate the variability during signal detection, we further arranged the V-shaped geometries within a compact spatial area so that all data points could be collected simultaneously. This compact arrangement not only improves the efficiency in data acquisition but also guarantees that all data is acquired at identical detection parameters. As a result, parallel and quantitative comparison among different sets of dose response experiments in a microdevice becomes possible. The following experiments highlighted the capability and flexibility of the microfluidic device in carrying out multiple sets of cell-based assays with single cell detection limit.

On-chip conditioning 1: single factor in various concentrations and time points

The dose-response and time-course effect of one single factor, calcein-AM (CAM, a viability stain, diffusion coefficient: 2.51×10^{-10} m^2 s^{-1} [17,18]), on individual cells was demonstrated by monitoring the fluorescence increment in cell cytoplasm (Fig. 3). Cell permeable CAM, a substrate of endogenous esterases, is subjected to enzymatic cleavage to give the fluorescent product, calcein.

Cells docked on the upper pipeline (*i.e.*, upper sandbag and upper gradient components) were exposed to increasing CAM concentrations (from right to left). Within 10 min, about 100 time-course responses were retrieved from the chronological images of individual cells (Fig. 3A, from top to bottom), while dose responses were derived from the collection of cells docked along the sandbag component (Fig. 3A, from right to left). The linearity of CAM time-course responses[34,35] was apparent among on-chip experiments (90% docked cells with $R^2 > 0.95$: selected data shown in Fig. 3B and tabulated in Table 2), suggesting that the assay environment offered by this microdevice was comparable to conventional assay conditions.

Kinetic profiles of the on-chip and conventional microplate experiments were fitted by Michaelis–Menten model[36] for comparison (Fig. 3C, see also Fig. S4 for reproducibility†).

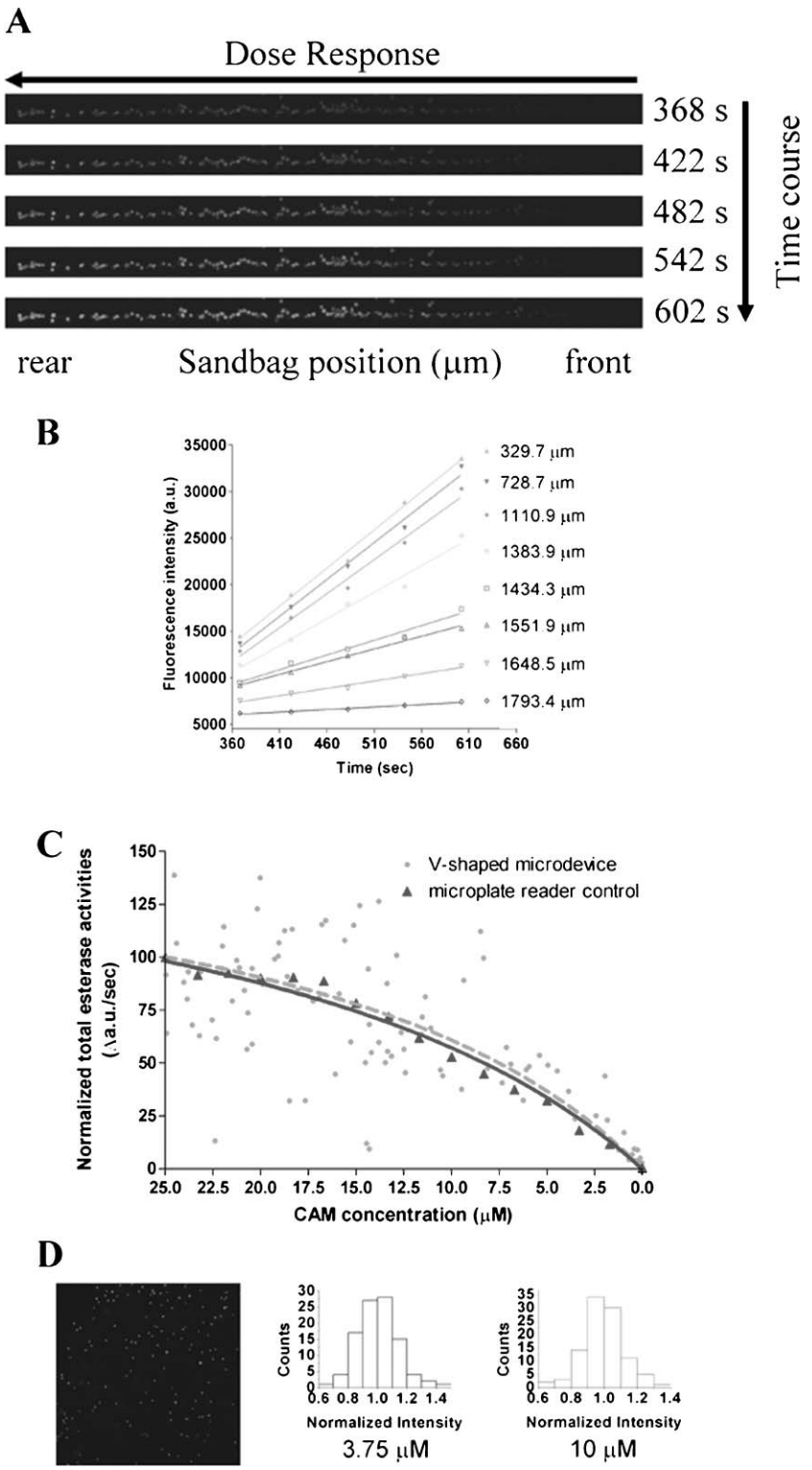

Fig. 3 On-chip analysis of a single factor CAM, with increasing concentrations from right to left, *i.e.*, from sandbag front to rear. (A) A series of confocal images showing CAM response intensity increased with respect to dosage and incubation time. (B) Time-course CAM response of individual cells showed good linearity, as illustrated in the selected single cells along the microchannel. Corresponding data were also tabulated in Table 2. (C) Normalized kinetic profiles of endogenous esterases retrieved from microdevice and microplate reader were compared. Similar profiles were observed in both experiments. (Each on-chip and microplate reader profile is the representative of three individual experiments, see also Fig. S4.†) (D) (Left) Confocal micrograph showing the origin of signal fluctuation in CAM stained cells. From the cells incubated with 3.75 μM (middle) and 10 μM (right) of CAM, 40% signal deviation could be observed.

Table 2 Linearity of CAM time-course responses

Distance coordinate/μm	CAM concentration/μM	Rate/a.u. s^{-1}	R^2
329.7	24.00	82.01	0.9945
728.7	19.40	79.39	0.9910
1110.9	15.20	73.22	0.9872
1383.9	7.55	57.00	0.9790
1434.3	6.47	31.65	0.9797
1551.9	3.87	27.35	0.9891
1648.5	1.99	15.91	0.9838
1793.4	0.29	5.44	0.9741

Although large scattering was observed from the response profile of the on-chip experiment, the Michaelis–Menten parameters retrieved from both methods were comparable (Table 3). As shown in Fig. 3D, when individual CAM experiments were conducted on glass slides with responses evaluated at single cell level (by confocal imaging), up to about 40% signal deviation was recorded. As every single cell is different, scattering is very common in bioassays. This intrinsic signal scattering was attributed to the proliferating cells (having higher esterase activity[37,38]) within a population. Since the measurement of microplate experiments was performed on an ensemble of cells, this signal scattering (noise) was actually smoothened. The microfluidics assay thus provides additional information at single cell level.

On-chip conditioning 2: two factors, both in various concentrations

The second example demonstrated the capability of superimposing two continuums of concentration gradients to study the interfering effects of two factors, TMR (tetramethylrosamine, diffusion coefficient: 4.79×10^{-10} m^2 s^{-1} [39,40]) and CAM. The first variables, differing doses of TMR, was applied to both upper and lower pipelines while the second variables, differing doses of CAM, was only applied to the lower pipeline.

Because of the compact data arrangement approach, it was possible to retrieve the upper and lower sets of TMR dose responses from a single confocal micrograph. As all single cell responses were captured simultaneously under identical focusing and detector parameters, direct and quantitative comparison of dose responses between upper and lower pipelines could be performed. Moreover, since the strongest (high concentration) and weakest (low concentration) signals were captured under the same window, detector parameters could be autoscaled to avoid saturation. As illustrated in Fig. 4B (see also Fig. S4† for reproducibility), it appeared that TMR dose response was not affected by the presence of differing doses of CAM. On the other hand, Fig. 4A showed the separated compartmentalization of the dyes in cytoplasm (light grey, CAM) and mitochondria (dark grey, TMR), indicating

Table 3 Comparison between microplate and on-chip experiment

	Microplate reader	On-chip experiment
	Best-fit	Best-fit
V_{max}	188.1 ± 12.64	176.1 ± 36.08
K_m	22.89 ± 2.96	18.94 ± 7.70

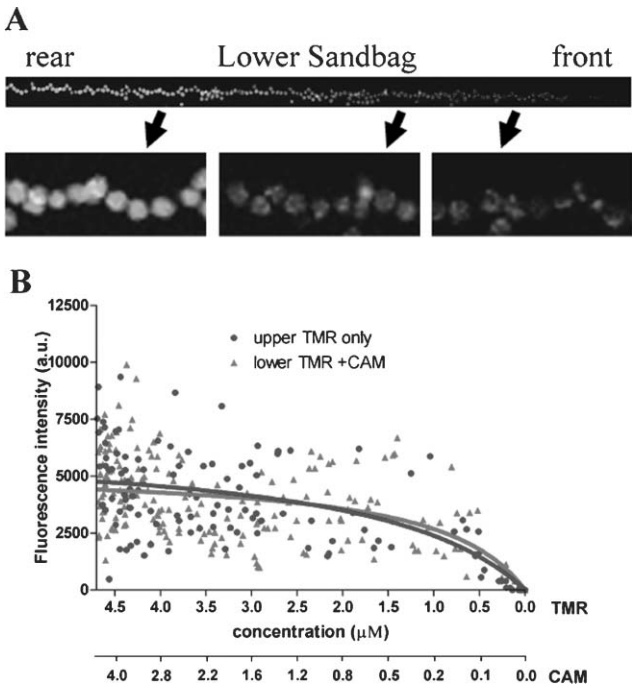

Fig. 4 On-chip comparative analysis of two factors: the first factor was TMR at various concentrations on both sandbag components. Another factor was CAM at various concentrations but exclusively applied on the lower sandbag. (A) Pseudocolored confocal image of the lower sandbag component. Facilitated by the compact data arrangement architecture, about 100 single cells treated with different analyte of gradient concentrations were captured simultaneously for direct comparison. The image was highly resolved that the mitochondria were clearly observed in the electronically enlarged view from the same image. (B) Quantitative comparison between the dose responses of cells on both sandbag components. No obvious interference was observed to TMR response in the presence of CAM at various concentrations.

parallel staining of cells with different dyes under different concentrations. Thus, the microfluidic device allows not only the treatment of an identical set of cells with different analytes of various gradient concentrations but also the comparison of responses with corresponding control experiments that were simultaneously conducted.

On-chip conditioning 3: two factors, one fixed while another in various concentrations

In the final example, the variable factor on both pipelines was the concentration of TMR. (TMR is a mitochondria stain[41,42] for cell viability as it fades out with the loss of mitochondria membrane potential.[43]) In addition, cells encompassed by the black dotted framework (Fig. 5A, top) were subjected to laser irradiation, which represented a constant factor for the cells on the upper pipeline. A confocal image was captured after applying the constant factor and the response intensities of the two pipelines were compared directly.

The on-chip result (Fig. 5A, bottom) showed some cells on the upper pipeline exhibited stronger fluorescence than the rest. Although identical TMR gradient was applied to both pipelines, the signal enhancement was only observed on the upper pipeline. There was a strong correlation between the

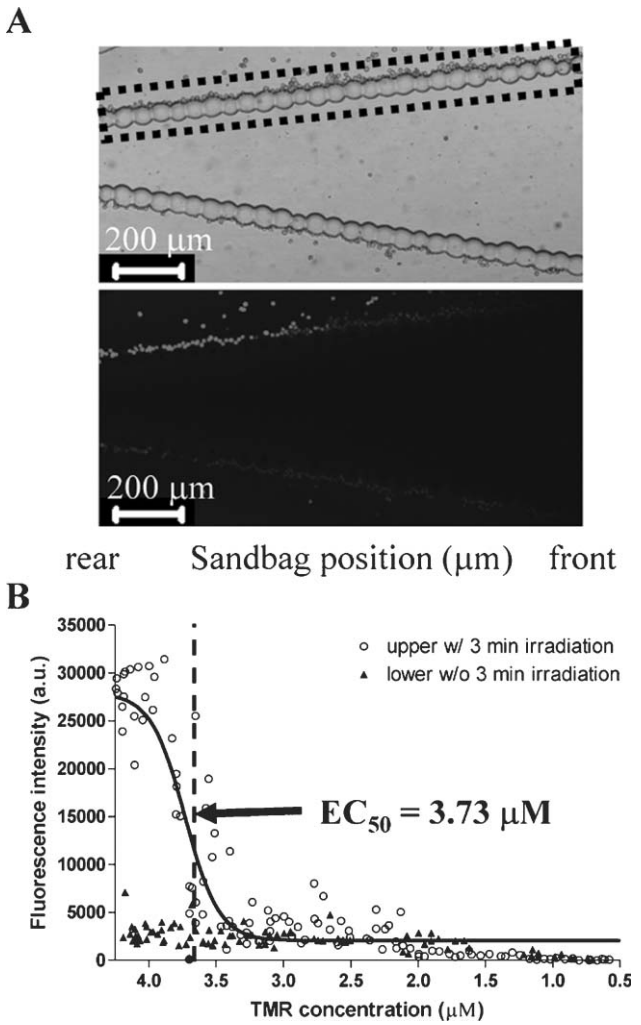

Fig. 5 On-chip comparative analysis between two factors: the fixed factor was the 3 min laser irradiation that was evenly but exclusively applied to the upper sandbag. Another factor, TMR gradient concentrations were applied over both sandbag components. (A) Compare TMR signal responses between the two pipelines with single cells: (Top) Bright-field confocal image illustrated the presence of cells on both sandbag components and only the region encompassed by the black dotted frame, was further exposed to 3 min laser irradiation. (Bottom) Identical confocal image: only cells exposed to both high TMR concentrations and 3 min irradiation exhibited signal enhancement. (B) Quantitative comparison between the dose response of cells on both sandbag components. EC_{50} of TMR required to trigger this signal enhancement was estimated to be 3.73 μM.

laser irradiation and the enhanced responses. It was also noted that this enhancement was only obvious to the cells incubated in high TMR concentrations, *i.e.*, near the sandbag rear. Therefore, it was concluded that the enhancement was a combined effect of (i) TMR concentration and (ii) laser irradiation. The EC_{50} of TMR concentration required for this enhancement was estimated to be 3.73 μM according to the dose response curve shown in Fig. 5B (see also Fig. S4 for reproducibility†). As fluorescence intensity was autoscaled due to the enhanced response triggered by the laser irradiation, the TMR signal scattering appeared to be less pronounced in Fig. 5B when compared with Fig. 4B (upper pipeline).

TMR and other photodynamic reagents[44] generate singlet oxygen when subjected to appropriate laser irradiation. The damage induced by singlet oxygen can be observed within minutes after light exposure and eventually triggers apoptosis.[45] Enhanced TMR signal in the above experiments indicated an increased dye uptake[46] due to membrane hyperpolarization during the apoptotic event of mitochondrial homeostasis.[47,48]

Conclusions

Using the advantages of geometric modulation of confined laminar streamlines, the throughput of the V-shaped microchannel was increased when comparing with its T-shaped analog. Further, we implemented a concept integrating a V-shaped geometry and a sandbag structure. Such a design provides a platform for conducting multiple sets of cell-based assays in parallel under different conditions. We have demonstrated the capability and flexibility of the design by fabricating two pipelines in a microdevice to simultaneously perform two sets of customized dose-dependent bioassays. The dual pipelines were arranged in close proximity to facilitate efficient and highly resolved image acquisition. The microdevice offered a stable yet controllable microenvironment to conduct experiments with minimal human interventions. Three sets of experiments were carried out to illustrate how factors of interest could be conditioned by the device to interrogate combined effects. Moreover, the microdevice was capable of providing quantitative data such as enzyme kinetic parameters and 50% effective concentration in a single microfluidic operation.

Acknowledgements

This work was supported by the Innovation and Technology Fund of Hong Kong SAR Government (ITS/015/02, CityU Project No. 9440026) and the National Hi-Tech 863 Program of the Ministry of Science and Technology of China (2003AA2Z2052).

References

1 A. Enomoto, M. C. Rho, A. Fukami, O. Hiraku, K. Komiyama and M. Hayashi, *Biochem. Biophys. Res. Commun.*, 2004, **323**, 1096.
2 P. C. H. Li and D. J. Harrison, *Anal. Chem.*, 1997, **69**, 1564.
3 M. S. Yang, C. W. Li and J. Yang, *Anal. Chem.*, 2002, **74**, 3991.
4 P. C. H. Li, L. de Camprieu, J. Cai and M. Sangar, *Lab Chip*, 2004, **4**, 174.
5 W. H. Huang, W. Cheng, Z. Zhang, D. W. Pang, Z. L. Wang, J. K. Cheng and Z. Zhang, *Anal. Chem.*, 2004, **76**, 483.
6 O. Kuksenok, J. M. Yeomans and A. C. Balazs, *Langmuir*, 2001, **17**, 7186.
7 A. D. Stroock, S. K. W. Dertinger, A. Ajdari, I. Mezic, H. A. Stone and G. M. Whitesides, *Science*, 2002, **295**, 647.
8 G. H. Seong and R. M. Crooks, *J. Am. Chem. Soc.*, 2002, **124**, 13360.
9 Y. Lin, G. J. Gerfen, D. L. Rousseau and S. R. Yeh, *Anal. Chem.*, 2003, **75**, 5381.
10 E. Leclerc, Y. Sakai and T. Fujii, *Biochem. Eng. J.*, 2004, **20**, 143.
11 W. Gu, X. Y. Zhu, N. Futai, B. S. Cho and S. Takayama, *Proc. Natl. Acad. Sci. U. S. A.*, 2004, **101**, 15861.
12 A. Tourovskaia, X. Figueroa-Masot and A. Folch, *Lab Chip*, 2005, **5**, 14.

13 J. G. Shackman, G. M. Dahlgren, J. L. Peters and R. T. Kennedy, *Lab Chip*, 2005, **5**, 56.
14 C. W. Li, C. N. Cheung, J. Yang, C. H. Tzang and M. S. Yang, *Analyst*, 2003, **128**, 1137.
15 A. P. Sudarsan and V. M. Ugaz, *Anal. Chem.*, 2004, **76**, 3229.
16 J. R. Anderson, D. T. Chiu, R. J. Jackman, O. Cherniavskaya, J. C. McDonald, H. K. Wu, S. H. Whitesides and G. M. Whitesides, *Anal. Chem.*, 2000, **72**, 3158.
17 W. J. Lyman, W. F. Reehl and D. H. Rosenblatt, *Handbook of Chemical Property Estimation Methods—Environmental Behavior of Organic Compounds*, American Chemical Society, Washington, DC, 1990.
18 R. H. Perry, D. W. Green and J. O. Maloney, *Perry's Chemical Engineers' Handbook*, McGraw-Hill, New York, 1997.
19 W. H. Gmeiner, C. J. Hudalla, A. M. Soto and L. Marky, *FEBS Lett.*, 2000, **465**, 148.
20 J. Yang, C. W. Li and M. S. Yang, *Lab Chip*, 2004, **4**, 53.
21 M. S. Yang, J. Yang, C. W. Li and J. L. Zhao, *Lab Chip*, 2002, **2**, 158.
22 A. R. Wheeler, W. R. Throndset, R. J. Whelan, A. M. Leach, R. N. Zare, Y. H. Liao, K. Farrell, I. D. Manger and A. Daridon, *Anal. Chem.*, 2003, **75**, 3581.
23 X. Y. Peng and P. C. H. Li, *Anal. Chem.*, 2004, **76**, 5273.
24 N. L. Jeon, H. Baskaran, S. K. W. Dertinger, G. M. Whitesides, L. Van de Water and M. Toner, *Nat. Biotechnol.*, 2002, **20**, 826.
25 M. A. McClain, C. T. Culbertson, S. C. Jacobson, N. L. Allbritton, C. E. Sims and J. M. Ramsey, *Anal. Chem.*, 2003, **75**, 5646.
26 G. Ocvirk, H. Salimi-Moosavi, R. J. Szarka, E. A. Arriaga, P. E. Andersson, R. Smith, N. J. Dovichi and D. J. Harrison, *Proc. IEEE*, 2004, **92**, 115.
27 S. Takayama, E. Ostuni, P. Leduc, K. Naruse, D. E. Ingber and G. M. Whitesides, *Nature*, 2001, **411**, 1016.
28 J. Gao, X. F. Yin and Z. L. Fang, *Lab Chip*, 2004, **4**, 47.
29 T. Li, H. W. Tang, M. N. Luo and G. Q. Chen, *Anal. Lett.*, 2004, **37**, 2053.
30 S. Takayama, J. C. McDonald, E. Ostuni, M. N. Liang, P. J. A. Kenis, R. F. Ismagilov and G. M. Whitesides, *Proc. Natl. Acad. Sci. U. S. A.*, 1999, **96**, 5545.
31 S. Takayama, E. Ostuni, X. P. Qian, J. C. McDonald, X. Y. Jiang, P. Leduc, M. H. Wu, D. E. Ingber and G. M. Whitesides, *Adv. Mater.*, 2001, **13**, 570–+.
32 J. Heo, K. J. Thomas, G. H. Seong and R. M. Crooks, *Anal. Chem.*, 2003, **75**, 22.
33 J. Voldman, M. L. Gray, M. Toner and M. A. Schmidt, *Anal. Chem.*, 2002, **74**, 3984.
34 Z. Hollo, L. Homolya, C. W. Davis and B. Sarkadi, *Biochim. Biophys. Acta*, 1994, **1191**, 384.
35 S. Hamann, J. F. Kiilgaard, T. Litman, F. J. varez-Leefmans, B. R. Winther and T. Zeuthen, *J. Fluoresc.*, 2002, **12**, 139.
36 T. Ngawhirunpat, N. Kawakami, T. Hatanaka, J. Kawakami and I. Adachi, *Biol. Pharm. Bull.*, 2003, **26**, 1311.
37 R. C. Flanigan, E. J. Pavlik, J. R. Vannagell, K. Keaton and D. E. Kenady, *J. Urol.*, 1986, **135**, 1091.
38 J. Uggeri, R. Gatti, S. Belletti, R. Scandroglio, R. Corradini, B. M. Rotoli and G. Orlandini, *Histochem. Cell Biol.*, 2004, **122**, 499.
39 B. O. Haglund, D. E. Wurster, L. O. Sundelof and S. M. Upadrashta, *J. Chem. Educ.*, 1996, **73**, 889.
40 C. T. Culbertson, S. C. Jacobson and J. M. Ramsey, *Talanta*, 2002, **56**, 365.
41 I. C. Summerhayes, T. J. Lampidis, S. D. Bernal, J. J. Nadakavukaren, K. K. Nadakavukaren, E. L. Shepherd and L. B. Chen, *Proc. Natl. Acad. Sci. U. S. A.*, 1982, **79**, 5292.
42 L. Villeneuve, P. Pal, G. Durocher, D. Migneault, D. Girard, R. Giasson, A. Balassy, L. Blanchard and L. Gaboury, *J. Fluoresc.*, 1996, **6**, 209.
43 W. M. Blom, H. J. G. M. De Bont and J. F. Nagelkerke, *J. Biol. Chem.*, 2003, **278**, 12467.
44 M. R. Detty, P. N. Prasad, D. J. Donnelly, T. Ohulchanskyy, S. L. Gibson and R. Hilf, *Bioorg. Med. Chem.*, 2004, **12**, 2537.
45 T. J. Dougherty, C. J. Gomer, B. W. Henderson, G. Jori, D. Kessel, M. Korbelik, J. Moan and Q. Peng, *J. Natl. Cancer Inst.*, 1998, **90**, 889.
46 J. Moan and T. Christensen, *Photobiochem. Photobiophys.*, 1981, **2**, 291.
47 M. G. Vander Heiden and C. B. Thompson, *Nat. Cell Biol.*, 1999, **1**, E209–E216.
48 G. Kroemer and J. C. Reed, *Nat. Med.*, 2000, **6**, 513.